Investigation of optoelectronic properties of half-Heusler KZnN and KZnP compounds

S. Azzi[a,b], F. Belkharroubi[c,d], N. Ramdani[a], M. Ameri[c], I. S. Messaoudi[a,e], W. Belkilali[f,g], L. Drici[c], L. Blaha[f], I. Ameri[c], Y. Al-Douri[h,i,j,*], and A. Bouhemadou[k]

[a]*Département de Génie Physique, (LPMF), Université des Sciences et de la Technologie d'Oran, Mohamed Boudiaf, Oran, Algeria.*

[b]*École Supérieure en Sciences Biologiques d'Oran (ESSBO), BP 1042, Saim Mohamed 31003, Oran, Algeria.*

[c]*Laboratory of Physical Chemistry of Advanced Materials, University of Djillali Liabes, BP 89, Sidi-Bel-Abbes 22000, Algeria.*

[d]*Genius Physics Department, Faculty of Physics, University of Sciences and Technology USTO-MB 31000, Oran, Algeria.*

[e]*Belhadj Bouchaib University Center, Ain Temouchent, Algeria.*

[f]*Physics Department, University of Ahmed Zabana, 48000, Relizane, Algeria.*

[g]*Applications of Plasma, Electrostatics and Electromagnetic Compatibility, Faculty of Technology, Djillali Liabes University, SidiBel Abbes, Algeria.*

[h]*Department of Applied Physics and Astronomy, College of Sciences, University of Sharjah, P.O. Box 27272, Sharjah, United Arab Emirates,*

[*]*e-mail: yaldouri@yahoo.com*

[i]*Department of Mechanical Engineering, Faculty of Engineering, Piri Reis University, EflatunSk. No:8, 34940 Tuzla, Istanbul, Turkey.*

[j]*Nanotechnology and Catalysis Research Centre, University of Malaya, 50603 Kuala Lumpur, Malaysia*

[k]*Laboratory for Developing New Materials and their Characterizations, Department of Physics, Faculty of Science, University Ferhat Abbas Setif 1, Setif, 19000, Algeria.*

Received 5 June 2022; accepted 4 June 2023

This is to investigate the structural, mechanical, electronic and optical properties of half-Heusler KZnN and KZnP compounds. The ab initio method based on density functional theory is employed. The study of structural properties has allowed us to verify the cubic structure type I that is the most stable among the three possible atomic arrangements for the two half-Heusler compounds. The mechanical stability is checked, since the calculated elastic constants obey the stability criteria of cubic. Our calculations have demonstrated that KZnN is a ductile material that is considerably stiffer than KZnP, which exhibits brittleness. The obtained results for the electronic properties with mBJ-GGA approximation reveal a semiconductor behavior with a band gap along Γ as estimated at 0.3 eV and 0.9 eV for KZnN and KZnP compounds, respectively. In addition, the optical properties have been studied by analyzing the variation of different parameters such as dielectric function, refractive index, reflectivity, absorption coefficient and conductance as a function of photon's energy for a wide range; 0 - 40 eV. The origin of peaks in the optical spectra is determined in terms of calculated energy band structures. This work has predicted strong absorption in the ultraviolet field.

Keywords: Half-Heusler; KZnN; KZnP; mechanical; optical.

DOI: https://doi.org/10.31349/RevMexFis.69.060501

1. Introduction

The researches in the field of materials have led to discover new materials for optoelectronic and solar cells applications, among which, Heusler compounds can be cited. Graft *et al*. [1] have represented detailed synthesis giving a broad overview of class of materials, not only on their nomenclature and their crystalline structures, but also on phenomena of order and disorder of magnetism. Heusler [2] had reported that a ferromagnetic alloy can be constructed from non-magnetic elements. He had discovered that the alloy with a composition Cu_2MnAl behaves like a ferromagnetic, although none of its constituent elements is magnetic. These materials constitute a premium package for many applications due to their various physical properties, so Bang *et al*. [3] have used Quick-Dipped method to make Cu_2MnAl Heusler alloy samples of different thicknesses. All samples

have exhibited mild magnetic behavior with a coercivity of less than 1.6 kA/m and high Curie temperature of around 600. Aniruddha Deb *et al*. [4] have studied the electronic structure and chemical bonding mechanism of Cu_2MnAl Heusler alloy using full-potential linearized augmented-plane-wave (FLAPW) method. They have found that their results are in good agreement with experimental data of ultraviolet photoemission spectroscopy. The magnetic Compton profiles (MCPs) have also been calculated. The spin moment on Mn site calculated to be 3.20 μB, is in agreement with value deduced from experimental profiles. Several researches have carried out in semi-metallic ferromagnetic alloys [5], in non-magnetic semiconductors [6] and even superconductors [7], as well as ferrimagnetics [8] and heavy fermion systems [9]. Heusler materials fall into three categories; quaternaries, full-Heusler and half-Heusler de Groot *et al*., [10] have discovered Heusler alloy of NiMnSb type.

For the new materials of various technological applications, the researchers have taken an interest in Heusler compounds, which occupy a prominent place. Depending on number of elements involved in composition of Heusler materials, there are two main families of compounds: ternary Heusler and quaternary Heusler [11]. A quaternary Heusler compounds have the composition XX'YZ. It can be broken down into four interpenetrating fcc sub-lattices X, X', Y and Y' that represent four types of sites; A (0,0,0), B (0.25,0.25,0.25), C (0.5,0.5,0.5) and D (0.75,0.75,0.75). The type of Heusler quaternary compounds (prototype LiMgPdSb) belongs to symmetry (space group no, 225) [3]. These quaternary Heusler compounds have very high technological performance due to having several behaviours. While, Ozdogan *et al.* [12] have studied Heusler quaternary compounds, where all the compounds are submitted according to Slater-Pauling rule, the behaviour of these materials are varied between half-metals, non-gapless semiconductors without spin, magnetic semiconductors and semiconductors. Among various works, Ayad *et al*. [13] have investigated magnetic and thermodynamic properties of new multifunctional full-Heusler alloy Co2TaGa using full-potential linear augmented plane waves (FP-LAPW) method. They have found that $CuHg_2$Ti-type structure FM phase is more stable for Co_2TaGa, and Co_2TaGa has half-metallic ferromagnetic with 100% spin polarization, with a magnetic moment of 2 μB. Half-Heusler is characterized by different behaviour, in fact they have found to be half-metallic magnets and the newly planned multifunctional topological insulators and recently, as suitable, adequate semiconductor materials intimately linked to the rapid and efficient development of optoelectronics [14]. Gruhn *et al.* [15] have extensively studied half-Heusler compounds with a large energy gap, which are mostly 8-electron half-Heusler compounds. The theoretical study is undertaking on half-Heusler compounds with 8 electrons using density functional density (DFT), which allowed to classify them according to five types; II-VI, I-II-V, I-III -IV, II-II-IV and II-III-III. So far, these materials have not been synthesized experimentally.

A great interest has been shown in half-Heusler semiconductors, which are exciting materials that find their place in new spintronics and optoelectronics technology. Particularly, the eight-electron half-Heusler class that includes a large number of semiconductors whose bandgaps vary over a wide range. Benzoudji *et al*. [16] have investigated the optoelectronic and thermoelectric properties of half-Heusler MRhSb (M = Ti, Zr, Hf), they have confirmed the stability in the cubic phase and highlighted their ductile nature. Electronic analysis has revealed their semiconducting nature with an indirect energy band gap ($\Gamma - X$). The evaluation of Seebeck coefficient has led to thermopower $S \geq 500$ μeV, which is very beneficial for thermoelectric applications.

Belmiloud *et al.* [17] have investigated systematic theoretical study of structural and electronic properties of new half-Heusler compounds; ScAgC, YCuC, CaZnC, NaAgO, and LiCuS. They have found a direct band gap close to 1 eV being quasi-lattice matched to GaAs (Si), and confirmed mechanical and dynamical stability of these compounds, which could be strong candidates for photovoltaic applications in multi-junction devices.

This work is devoted for studying the two half-Heusler KZnN and KZnP compounds, which belong to I-II-V family, using density functional theory (DFT) [18]. These two materials have been subjected to structural and electronic studies by Gruhn *et al*. [19], Kacimi *et al*. [20] and Kieven *et al*. [21]. Liu *et al*. [22] and Mehnane *et al*. [23] have conducted studies on thermal and electrical transport properties of KZnP. We have investigated more in-depth studies of half-Heusler KZnN and KZnP compounds, by focusing on structural, electronic properties and verifying their mechanical stability through calculating the elastic constants. To our knowledge, it is not available in the literature this study yet. In addition to the optical properties, we have conducted a detailed analysis of various optical quantities; dielectric function, refractive index, reflectivity, absorption coefficient and conductance. KZnN and KZnP compounds have a formula XYZ and crystallize in non-centrosymmetric cubic structure (space group No. 216, $F\bar{4}3m$). The half-Heusler structure can be viewed as ZnS-sublattice (Wyckoff positions 4a (0,0,0), and 4c (1/4,1/4,1/4)) in which the octahedral sites are occupied 4b (1/2,1/2,1/2) [24]. This paper is divided into the followings; Section 2 describes the calculation method. The obtained results obtained are elaborated in Sec. 3. Finally, the conclusions are outlined in Sec. 4.

2. Computational

The calculations are performed with *ab initio* method based on functional density theory (DFT) [18] of full-potential linearized augmented plane-wave (FP-LAPW) method [25], implemented in WIEN2k package [26,27]. The generalized gradient approximation (GGA) [28] is used to determine the structural and elastic properties, whereas for the calculation of electronic and optical properties are achieved utilizing the modified Becke-Johnson approximation (mBJ-GGA) [29].

In order to separate the core and valence states, the cut-off energy, -6 Ryd is used. Within the muffin-tin spheres, all basic functions have been extended up to $R_{MT}K_{MAX} = 8$ (R_{MT} is the muffin-tin radius, K_{MAX} is the maximum modulus of the reciprocal lattice vectors). The expansion of spherical harmonics inside atomic spheres and plane waves in the interstitial regions are limited to maximum quantum number $l_{\max} = 10$. For self-consistent calculations, the energy and charge convergence are set to be 0.0001 Ryd and 0.001, respectively. The k-space integration on first Brillouin zone (BZ) for self-consistent calculations is performed with $14 \times 14 \times 14$ k-point Monkhorst-Pack (MP) mesh [30].

3. Results and discussion

3.1. Structural properties

Half-Heusler compounds of KZnN and KZnP are crystallizing in the cubic face-centered structure (Space group: F$\bar{4}$3m), where the K atoms are positioned at (0.25,0.25,0.25), Zn atoms at (0.0,0.0,0.0) and N and P atoms at (0.5,0.5,0.5), by swapping between these positions three types of arrangements are obtained, namely types I, II and III. Figure 1 shows the variation of total energy as a function of volume, it is seen that the cubic type I has the lowest energy among the three types. The lattice constants and bulk modulus are determined by fitting the total energy versus volume to Murnaghan's equation of state [31] using the generalized gradient approximation (GGA) [28]. The results concerning these parameters plus the bulk modulus pressure derivative of KZnN and KZnP compounds are compared with other theoretical results as given in Table I. The results allow us to conclude:

- The cubic structure type I is the most stable among the three possible atomic arrangements for the two half-Heusler.
- When the N atom is replaced by P atom, an increasing in the value of lattice parameter and a decreasing in the value of mass modulus are observed.
- The results are in good agreement with the available in literature for the cubic structure type I [20,21,23].
- In the absence of experimental results, only one result is found for KZnP in the hexagonal structure P63/mmc [32], these results remain predictive.

3.2. Mechanical properties

The elastic constants $\mathbf{C}_{ij}$ are obtained by the calculation of total energy according to conservation of the strains by Mehl [33] method, the elastic modules require the knowledge of derivative of energy according to strain of crystal lattice. For the cubic system, the corresponding mechanical stability criteria [34,35] are:

$$\mathbf{C}_{11} + 2\mathbf{C}_{12} > 0, \quad \mathbf{C}_{11} - \mathbf{C}_{12} > 0$$
$$\mathbf{C}_{11} > 0, \quad \mathbf{C}_{44} > 0. \tag{1}$$

The first equation consists in calculating the modulus of compressibility B, which is linked to elastic constants by the following [36]:

$$B = \frac{(\mathbf{C}_{11} + 2\mathbf{C}_{12})}{3}. \tag{2}$$

Other quantities linked to elastic constants such as Young's modulus E:

$$E = \frac{(\mathbf{C}_{11} - \mathbf{C}_{12})(\mathbf{C}_{11} + \mathbf{C}_{12})}{(\mathbf{C}_{11} + \mathbf{C}_{12})}. \tag{3}$$

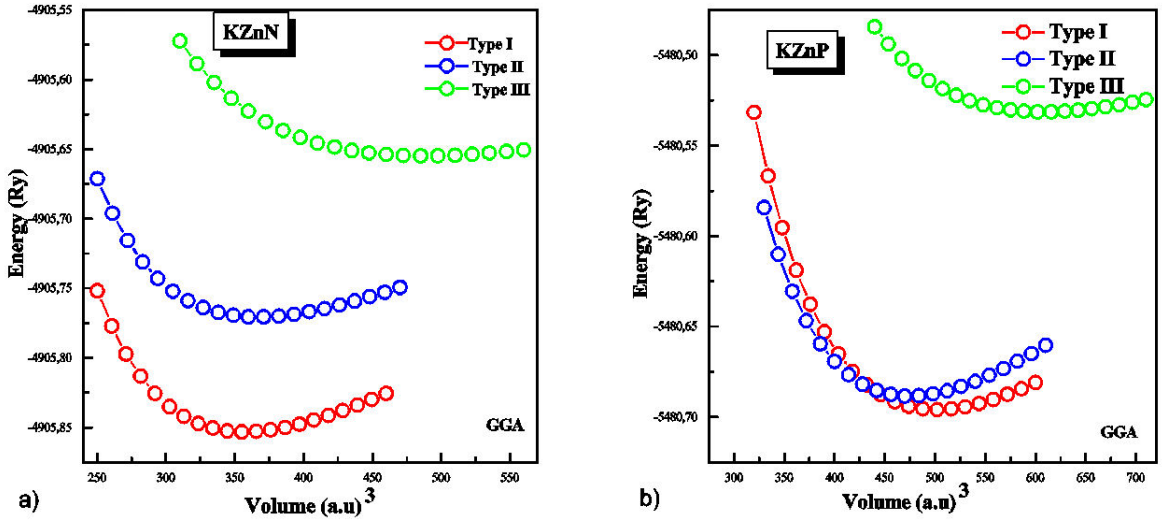

FIGURE 1. Total energy as a function of volume for type I, type II and type III of a) KZnN, and b) KZnP compounds.

TABLE I. The calculated structural parameters of KZnN and KZnP compounds such as equilibrium lattice constant a(Å), bulk modulus B(GPa), its pressure derivative B' and total energy, using GGA approximation.

	Type		a(Å)	B(GPa)	B'	$E_{\min}$(Ry)
KZnN	Type I	Present work.	5.961	45.331	4.938	-4905.853147
	Type II	Present work.	6.013	35.962	4.748	-4905.770545
	Type III	Present work.	6.615	15.544	4.672	-4905.654774
		Other theo.	5.962[a]			
			5.960[b]			
			5.963[c]	46.374[c]	4.283[c]	
				5.959[d]		
KZnP	Type I	Present work.	6.674	31.709	4.513	-5480.695895
	Type II	Present work.	6.553	35.167	4.255	-5480.688485
	Type III	Present work.	7.119	15.774	4.538	-5480.531289
		Other theo.	6.674[a]			
			6.674[c]	32.521[c]	4.146[c]	
			6.673[d]			

[a]Ref. [20] GGA, [b]Ref. [20] PBE-GGA, [c]Ref. [23], [d]Ref. [21].

TABLE II. Values of the elastic constants C_{ij} calculated (GPa), and the bulk modulus B (calculated from C_{ij}), for the type I cubic structure of the KZnN and KZnP compounds.

	C11	C12	C44	B
KZnN	129.835	3.503	010.878	45.620
KZnP	58.397	17.504	22.105	31.140

TABLE III. Calculated the Young modulus E (GPa), the shear modulus G (GPa), the Poisson's ratio η, the (B/G) ratio and the Zener anisotropy factor A for the cubic simple structure, of KZnN and KZnP compounds.

	E	G	η	B/G	A
KZnN	129.651	24.028	0.276	1.898	0.172
KZnP	50.318	21.426	0.220	1.453	1.081

The shear modulus G, Voigt shear modulus G_V, and Reuss shear modulus G_R are obtained by [37-39]:

$$G = \frac{G_V + G_R}{2}, \tag{4}$$

$$G_V = \frac{\mathbf{C}_{11} - \mathbf{C}_{12} + 3\mathbf{C}_{44}}{5}, \tag{5}$$

$$G_R = \frac{5(\mathbf{C}_{11} - \mathbf{C}_{12})\mathbf{C}_{44}}{4\mathbf{C}_{44} + 3(\mathbf{C}_{11} - \mathbf{C}_{12})}. \tag{6}$$

The Poisson coefficient η [40]:

$$\eta = \frac{3B - 2G}{2(3B + G)}. \tag{7}$$

The Zener anisotropy factor A can be deduced according to following [37-39]

$$A = \frac{2\mathbf{C}_{44}}{(\mathbf{C}_{11} - \mathbf{C}_{12})}. \tag{8}$$

In order to confirm the mechanical stability of KZnN and KZnP compounds, the constants $\mathbf{C}_{ij}$ in cubic structure are calculated and presented in Table II. As well as the compressibility modulus B (calculated from $\mathbf{C}_{ij}$). The values of elastic constants are found and match the mechanical stability criteria mentioned above [34,35]. An important remark is that the value of compression modulus B calculated from the formulas is close to that obtained by the optimization. Different mechanical quantities of KZnN and KZnP half-Heusler compounds are calculated such as the Young's modulus E, shear modulus G and coefficient of Poisson η, the Zener anisotropy factor A and B/G ratio, these different parameters are displayed in Table III. These results are in very good agreement with Voigt-Reuss approximation.

Table III presents the value of Young's modulus of KZnN that is greater than KZnP, which leads to deduce that KZnN is much more rigid than KZnP. The value of Poisson's ratio η tells us about characteristics of bonding forces that is a measure of compressibility, is defined by a relationship between

TABLE IV. Band gap E_g (eV) calculated using both GGA and mBJ-GGA approaches for half-Heusler KZnN and KZnP compounds.

		E_g ($\Gamma - \Gamma$)		
		GGA	mBJ- GGA	TB-mBJ
KZnN	Present work	0	0.30	
	Other theo.	$0^{a,c}$	0.297^{a}	0.30^{b}
KZnP	Present work	0	0.90	
	Other theo.	$0^{a,c}$	0.949^{a}	

[a,b]Ref. [20], [c]Ref. [21].

lateral and longitudinal deformation in uniaxial tensile stress. This ratio determines the bonding nature, and its value varies in different materials. For covalent materials, $\eta = 0.1$, for ionic materials, $\eta = 0.25$ and for metal, $\eta = 0.33$ [41]. The values obtained from the Poisson's ratio are 0.276 for KZnN and 0.22 for KZnP, are close to value corresponding to ionic materials, which shows ionic character of these materials.

The ductile and brittle responses of materials represent two important mechanical characteristics of solids when exposed to external deformation. A material is considered ductile if its B/G ratio is greater than 1.75, otherwise it becomes brittle [36]. The calculated B/G values are 1.898 for KZnN and 1.453 for KZnP, thus, KZnN is a ductile material, while KZnP is brittle. The Zener anisotropy factor A indicates a degree of elastic anisotropy of crystal. Any value less or greater than 1 indicates an anisotropy characteristic. From the results obtained in Table III, it is possible to deduce an elastic anisotropic nature of these materials, and KZnN is much more anisotropic than KZnP.

3.3. Electronic properties

3.3.1. *Band structure*

Figures 2a) and 3a) illustrate the electronic band structures of KZnN and KZnP compounds, respectively, calculated at equilibrium lattice parameters with mBJ-GGA [29] approach, along high symmetry directions in the first Brillouin zone. Using the mBJ-GGA approximation, which aims to improve the null values of gaps obtained with GGA, direct band gap ($\Gamma - \Gamma$), 0.30 eV for KZnN and 0.90 eV for KZnP have been found, which shows the semiconductor aspect of these materials. These results are in good agreement with previous results [20,21] as displayed in Table IV.

3.3.2. *Density of states*

The density of states of a solid can be defined as a distribution of electronic states of system as a function of energy. The electronic density of states (total and partial) using mBJ-GGA can be shown in Fig. 2b) and 4 for KZnN, and in Figs. 3b) and 5 for KZnP. From the previous figures, it is found at bottom of valence region between -10 eV and -5 eV, the Zn-d states mainly contribute for both materials, with both peaks being detected at -6 eV. The top of valence

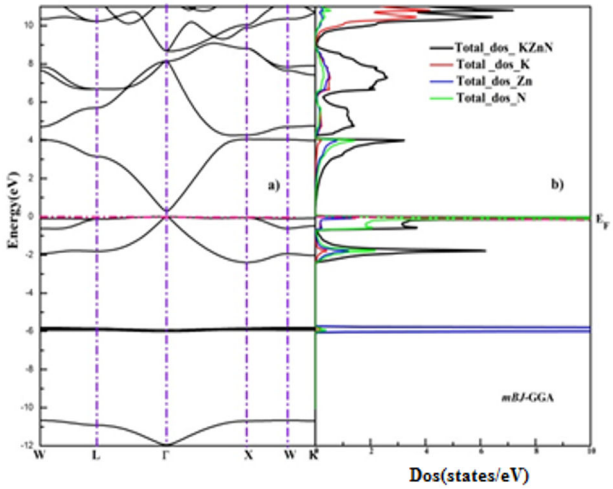

FIGURE 2. a) Band structure and b) total state densities of the KZnN compound with the mBJ-GGA.

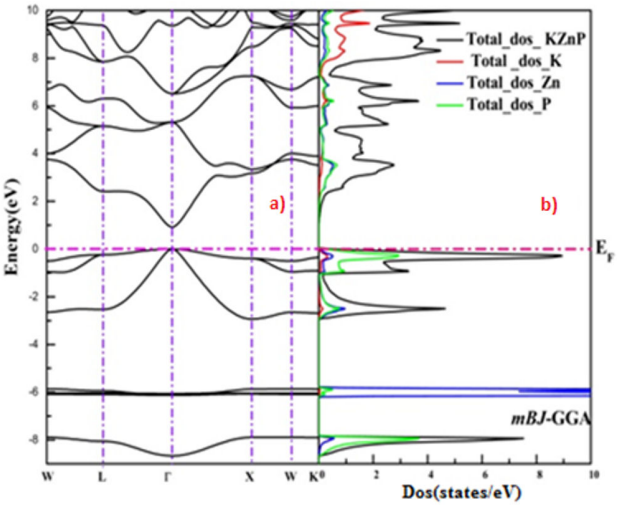

FIGURE 3. a) Band structure and b) total state densities of the KZnP compound with the mBJ-GGA.

band between -5 eV and 0 eV is characterized by a strong contribution of N-p states for KZnN and P-p states for KZnP, both near the Fermi level.

The bottom of conduction band between 0 eV and 5 eV is characterized by a very weak contribution of Zn-s and N-p states for KZnN, the contribution of P-p and Zn-s states is as

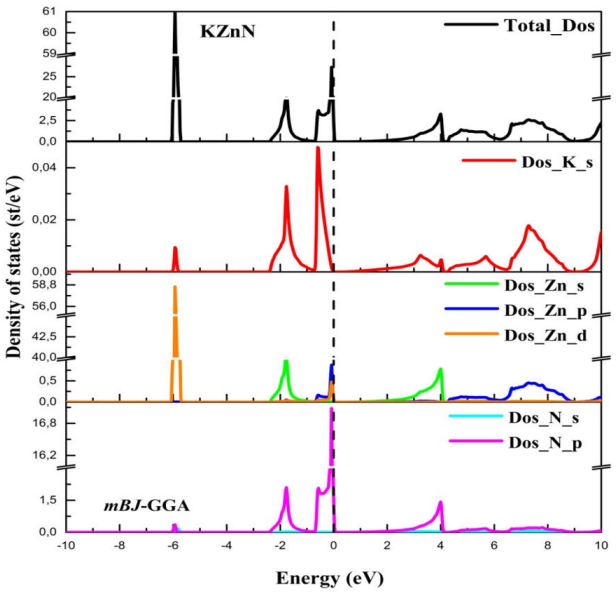

FIGURE 4. Total and partial state densities of the KZnN compound with the mBJ-GGA.

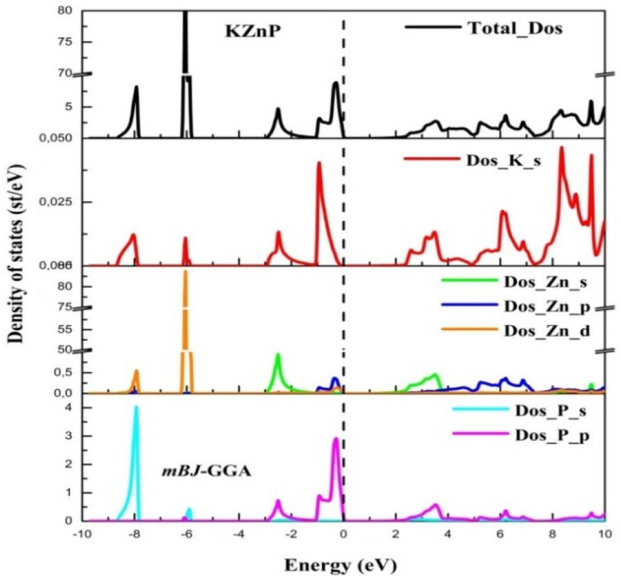

FIGURE 5. Total and partial state densities of the KZnP compound with the mBJ-GGA.

weak for KZnP, similarly, the top of conduction band is characterized by a weak contribution, Zn-p and N-p states for KZnN, same weak contribution for Zn-p and P-p states for KZnP.

3.3.3. Optical properties

The study of optical properties of materials allows us to understand the phenomena of interaction of luminous radiation with matter, in particular the interaction of photons with solid. For this purpose, the optical properties of both half-Heusler KZnN and KZnP compounds, such as dielectric function, refractive index, reflectivity, absorption coefficient and conductivity are investigated.

3.3.3.1 The dielectric function

The dielectric function of a crystal is defined by the transitions between the valence bands and conduction bands. In static field's case, the dielectric function is a real quantity, however it is a complex function in case of dynamic field. It is written as follows:

$$\varepsilon(\omega) = \varepsilon_1(\omega) + i\varepsilon_2(\omega), \tag{9}$$

where $\varepsilon_1(\omega)$ is real part and $\varepsilon_2(\omega)$ is imaginary part of dielectric functions. The $\varepsilon_1(\omega)$ depends on $\varepsilon_2(\omega)$. The expression of $\varepsilon_1(\omega)$ is given by Kramers-Kronig transformation [42-44]:

$$\varepsilon_1(\omega) = 1 + \frac{2}{\pi}\int_0^{\infty} \frac{\omega'\varepsilon_2(\omega')}{\omega'^2 - \omega^2} d\omega'. \tag{10}$$

The $\varepsilon_2(\omega)$ is given according to perturbation theory [45]:

$$\varepsilon_2(\omega) = \frac{4\pi^2 e^2}{3m^2\omega^2} \sum_{l,n} \int_{BZ} \frac{2}{(2\pi)^3} d^3k \mid P_{nl} \mid^2 \times \delta[E_1(k) - E_n(k) - \hbar\omega], \tag{11}$$

where w is frequency and P_{nl} represent elements of matrix moment. The curves represent real part of dielectric function of two KZnN and KZnP compounds that have been illustrated in Fig. 6a), b). From these curves, it is possible to determine the limit value $\varepsilon_1(0)$ for each material. That value corresponds to an irradiation frequency close to zero designated by static dielectric constant. The results obtained of $\varepsilon_1(0)$ for KZnN and KZnP compounds are 9.152 and 8.379, respectively. The curves of two compounds show roughly the same shape, except that the dielectric function reaches much lower negative values for KZnN than KZnP. These curves can be subdivided into:

i **The first region:** $\varepsilon_1(\omega)$ reaches several peaks distributed over an energy range from $0 - 3.3$ eV. The highest peaks; 10.64 for KZnN and 15.63 for KZnP are located at energy points 0.35 eV and 2.67 eV, respectively.

ii **The second region:** $\varepsilon_1(\omega)$ shows a sharp decrease reaching an important negative value, -10.46 for KZnN and less important one, -03.17 for KZnP. This decreasing is interpreted by the fact that photons are damped (damping of electromagnetic waves), then $\varepsilon_1(\omega)$ quickly increases back to positive values where it starts fluctuating until reaching 25.57 eV for KZnN, whereas for KZnP the fluctuations start earlier at negative values then proceed to positive ones until 23.74 eV. The positive variation of dielectric function explains that photons propagate through the compound.

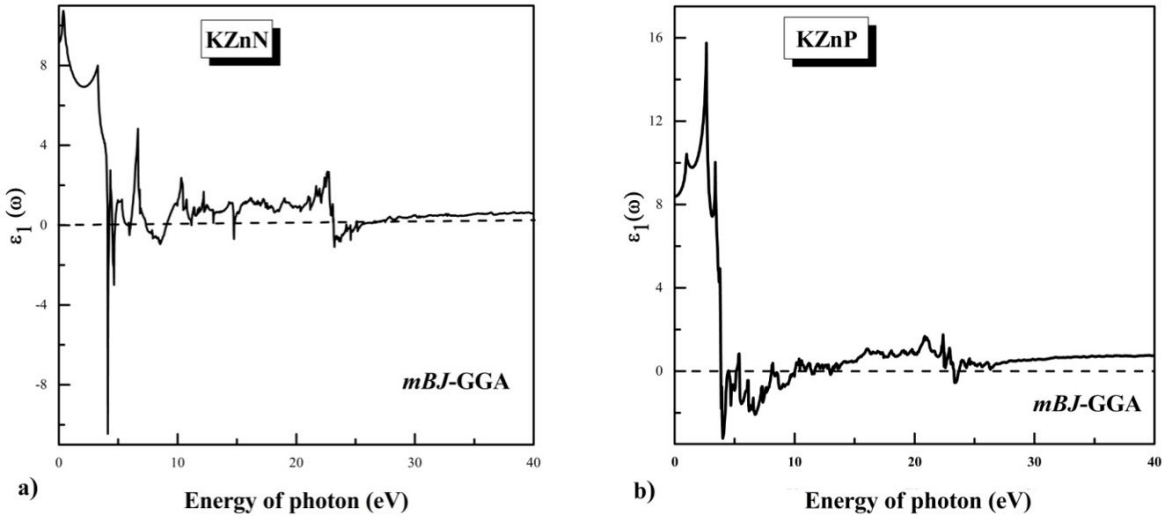

FIGURE 6. Real part $\varepsilon_1(\omega)$ of dielectric function for compounds a) KZnN b) KZnP with mBJ-GGA.

iii **The third region:** $\varepsilon_1(\omega)$ shows a slight increasing then a stabilization near zero at energies greater than 25.57 eV for KZnN and 23.74 eV for KZnP.

The $\varepsilon_2(\omega)$ is directly linked to structure of electronic band in a solid as represented on both right sides of Figs. 7 and 8 for KZnN and KZnP compounds, respectively. The absorption begins at energy 0.286 eV for KZnN and 0.939 eV for KZnP. Absorption peaks have been determined for each compound; these correspond to electronic transitions from valence states to conduction states. Analysis of peaks of $\varepsilon_2(\omega)$ for two half-Heusler reveals that critical points E_0 that represent the edge of optical absorption are 0.776 eV and 1.510 eV for KZnN and KZnP compounds, respectively, gives the threshold of direct optical transition between the topmost valence band V_1 and the bottommost conduction band C_1 (V_1-C_1 transition); while the second peaks E_1 are at 3.306 eV for KZnN and 2.680 eV for KZnP. From these curves, which reflect the absorption, different inter-band transitions (V_i-C_j) from the occupied valence state V_i to the empty conduction state C_j can be obtained [46]. The positions of main peaks E_i with the dominant contributions of interband transitions at each peak and at their positions in the first Brillouin zone of KZnN and KZnP compounds have been listed in Tables V and VI, respectively.

On the left side of Fig. 7, using six bars of red color, some main transitions of KZnN relating to E_1 peak with an energy value, 3.306 eV have been indicated. In W-L region, the first three bars have been represented, the 1st bar corresponds to direct transition energy V_1-C_1 of value 4.042 eV between the highest valence band V_1 and lowest conduction band C_1. The 2nd bar represents a direct transition energy V_2-C_1 of 4.648 eV, V_2 being the 2nd descending valence band. The 3rd bar represents the direct transition energy V_1-C_1 in L of 3.150 eV. The other bars are in X-W-K, the 4th bar represents the direct transition energy V_1-C_1 in X, of 4.049 eV, the 5th bar represents the direct transition energy V_1-C_1 near K, of 3.961 eV, and the 6th bar represents the direct transition en-

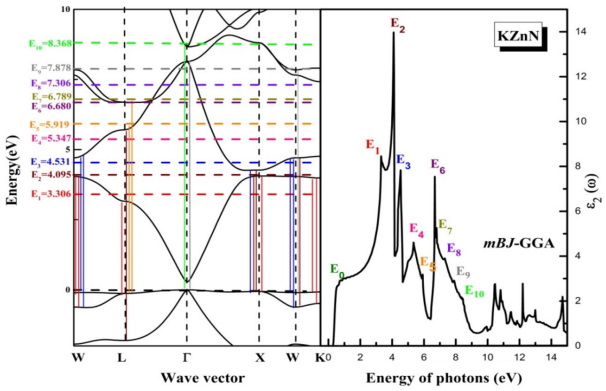

FIGURE 7. On the left side: Representation of some transitions energies band structure for KZnN compound, and on the right side: Imaginary part $\varepsilon_2(\omega)$ of dielectric function for KZnN compound with mBJ-GGA.

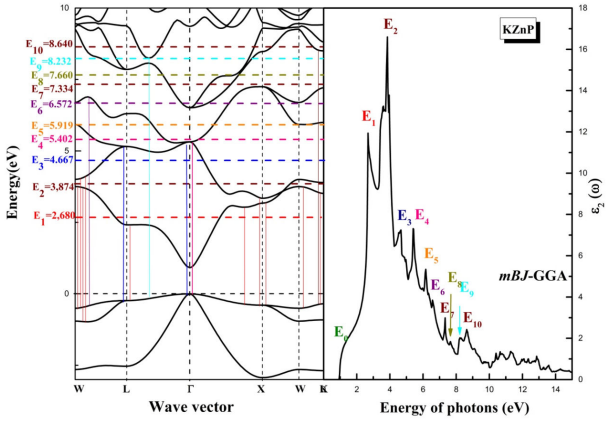

FIGURE 8. On the left side; Representation of some transitions energies band structure for KZnP compound, and on the right side; Imaginary part $\varepsilon_2(\omega)$ of dielectric function for KZnP compound with mBJ-GGA.

TABLE V. Optical transitions of KZnN compound in eV.

Optical structures		Dominant interband transition contributions		
Structure	Peak position (eV)	Transitions	Region	Energy(eV)
E_0	0.776	V_1-C_1	$\Gamma - \Gamma$	0.300
E_1	3.306	V_1-C_1	W-L	4.042, 3.150
			X-W-K	4.049, 3.961
		V_2-C_1	W-L	4.648
			X-W-K	4.442
E_2	4.095	V_1-C_1	W-L	4.086, 3.175
			X-W-K	4.086, 3.986
		V_1-C_2	W-L	4.710 , 5.316
			X-W-K	4.273, 4.710, 4.760
E_3	4.531	V_1-C_2	W-L	4.685, 5.721
			Γ-X-W-K	4.274, 4.710, 5.316
E_4	5.347	V_1-C_2	W-L	4.23, 5.721, 5.354
			W-K	4.710, 4.748
E_5	5.919	V_1-C_2	W-L-Γ	4.042, 3.150
			W-K	4.698
		V_1-C_3	W-L-Γ	6.707
			W-K	7.668
E_6	6.680	V_1-C_3	W-L-Γ	7.668, 6.695
E_7	6.789	V_1-C_3	W-L-Γ	7.656, 6.707, 6.801
			W-K	7.655, 7.431
E_8	7.306	V_1-C_2	L-Γ	8.142
		V_1-C_3	X-L-Γ	7.655, 6.707,6.682,8.142
			W-K	7.656, 7.631
		V_1-C_4	X-W-Γ	7.867
			W-K	7.868,7.893
E_9	7.878	V_1-C_2	L-Γ	8.167
			X-L-Γ	7.656, 6.682,8.167
		V_1-C_3	X-W-K	7.381
			X-L-Γ	7.868, 8.167
		V_1-C_4	X-W-K	7.893
E_{10}	7.878	V_1-C_2	W-L-T	8.167
		V_1-C_3	W-L-Γ	7.655, 8.249
			X-W-K	7.381, 8.287, 7.406
		V_1-C_4	W-L-Γ	7.868, 8.462
			X-W-K	8.816, 7.855, 7.918, 8.486
		V_1-C_5	Γ- X	8.666

TABLE VI. Optical transitions of KZnP compound in eV.

Optical structures		Dominant interband transition contributions		
Structure	Peak position (eV)	Transitions	Region	Energy(eV)
E_0	1.510	V_1-C_1	$\Gamma - \Gamma$	0.900
E_1	2.680	V_1-C_1	W-L	3.742, 2.673
			Γ-X	3.162
			X-W-K	3.565, 4.484,4.490
		V_1-C_2	W-L	4.502
			Γ-X	4.484
		V_2-C_1	W-L	4.649
		V_2-C_2	W-L	5.083
E_2	3.850	V_1-C_1	W-L	3.742, 4.225
			X-W-K	4.053, 3.499
		V_1-C_2	W-L	4.027
			Γ-X	3.370, 3.757
			X-W-K	3.742, 3.898
E_3	4.667	V_1-C_2	W-L-Γ	4.019, 4.501, 5.153, 5.300
			W-K	4.01, 3.932
		V_1-C_3	W-L-Γ	5.923, 6.406, 6.304, 6.544, 5.317
E_4	5.402	V_1-C_3	W-K	5.923, 5.992
			W-L-Γ	5.923, 6.388
E_5	5.919	V_1-C_4	W-L-Γ	6.304, 6.544
			W-k	5.931, 6.405, 6.018, 6.362
E_6	6.572	V_1-C_4	W-L-Γ	6.676, 7.176, 6.330, 6.570
		V_1-C_5	W-k	6.702, 7.202, 7.178, 7.548
E_7	7.334	V_1-C_5	Γ-X	7.264
			X-K	7.594, 7.265
		V_1-C_6	Γ-X	7.862, 8.102
			X-K	7.204
E_8	7.660	V_1-C_6	L-Γ	7.862, 8.078
			Γ-X	7.680
E_9	8.232	V_1-C_6	W-L-Γ	7.862, 8.070, 8.085
			X-K	8.477, 8.503
		V_1-C_7	L-Γ	8.251
E_{10}	8.640	V_1-C_6	W-L-Γ	9.022
			X-K	8.477, 8.503
		V_1-C_7	X-K	8.814
		V_1-C_8	L-Γ	8.252

ergy V_2-C_1 near K, estimated at 4.442 eV. The other bars of different colors each correspond to the energy peaks noted with same color on the right side of Fig. 7. For KZnP, the main transitions relating to peak E_1 of 2.680 eV have been represented by ten bars of red color, on the left side of Fig. 8. In the W-L, five bars have been represented, the 1st bar corresponds to the direct transition energy V_1-C_1 of 3,742 eV, between the highest valence band V_1 and lowest conduction band C_1. The 2nd bar represents a direct transition energy V_1-C_2 of 4.502 eV, C_2 being the 2nd conduction band going upwards. The 3rd bar represents direct transition energy V_2-C_1 of 4.649 eV, the 4th bar represents the direct transition V_2-C_2 of 5.083 eV. Finally, the 5th bar at point of high symmetry L, represents a direct transition energy V_1-C_1 of 2.673 eV. In the $\Gamma - X$, there are two bars, one of direct transition V_1-C_1 of 3.162 eV and other of direct transition V_1-C_2 of 4.484 eV. Last, in the X-W-K, there are three bars, the 1st bar is at point X, of direct transition energy V_1-C_1 of 3.565 eV, the 2nd bar is near W, of direct transition energy V_1-C_1 of 4.484 eV and the 3rd direct transition bar is V_1-C_1 near K of 4.490 eV. The other bars of different colors each correspond to energy of peak noted with same color on the right side of Fig. 8.

3.3.3.2 The refractive index

Another complex quantity linked to ε, is the complex refractive index $N(w)$. The refractive index of a medium describes how light propagates:

$$N(w) = n(\omega) + ik(\omega). \tag{12}$$

The real part is given by:

$$n(\omega) = \frac{1}{\sqrt{2}}([\varepsilon_1(\omega)^2 + \varepsilon_2(\omega)^2]^{1/2} + \varepsilon_1(\omega))^{1/2}, \tag{13}$$

where n is the refractive index. The imaginary part is given by:

$$k(w) = \frac{1}{\sqrt{2}}([\varepsilon_1(\omega)^2 + \varepsilon_2(\omega)^2]^{1/2} - \varepsilon_1(\omega))^{1/2}, \tag{14}$$

where k is extinction coefficient. From the curves of Figs. 9a), b), we can read the values of static refractivity index at frequency 0, $n(0)$, which corresponds to 3.025 for KZnN and 2.895 for KZnP. The refractive index curves have the same trend for both compounds, in low energy region, they reach high peaks of 3.28 at 0.42 eV for KZnN and 4.13 at 2.74 eV for KZnP. Then, they show more moderate peaks with a lot of fluctuations, in the region between 10 eV and 25 eV. Finally, they stabilize near 0.75 in the interval; $25 - 40$ eV; for two compounds. The extinction coefficient $k(\omega)$, in Figs. 10a), b), reaches a maximum value, 3.64 that corresponds to 4.12 eV for KZnN, and a maximum value, 2.83 that corresponds to 3.88 eV for KZnP. These results concur with the values of the energies, which cancel the real parts of the dielectric function, since $\varepsilon_1(4.10) = 0$ for KZnN and $\varepsilon_1(3.87) =$0 for KZnP of Figs. 6a), b).

3.3.3.3 Reflectivity

Reflectivity is one of the important factors that describe the optical response of solids, it is defined as the ratio of intensity of reflected ray to intensity of incident ray at normal incidence of electromagnetic wave on the system, it is written as:

$$R(\omega) = \frac{(n-1)^2 + k^2}{(n+1)^2 + k^2}, \tag{15}$$

where n and k are real and imaginary parts of complex refractive index, respectively. Figure 11a), b) illustrates the spectral variation of reflectivity for the KZnN and KZnP compounds as a function of photonic energy. It is noticeable that the static

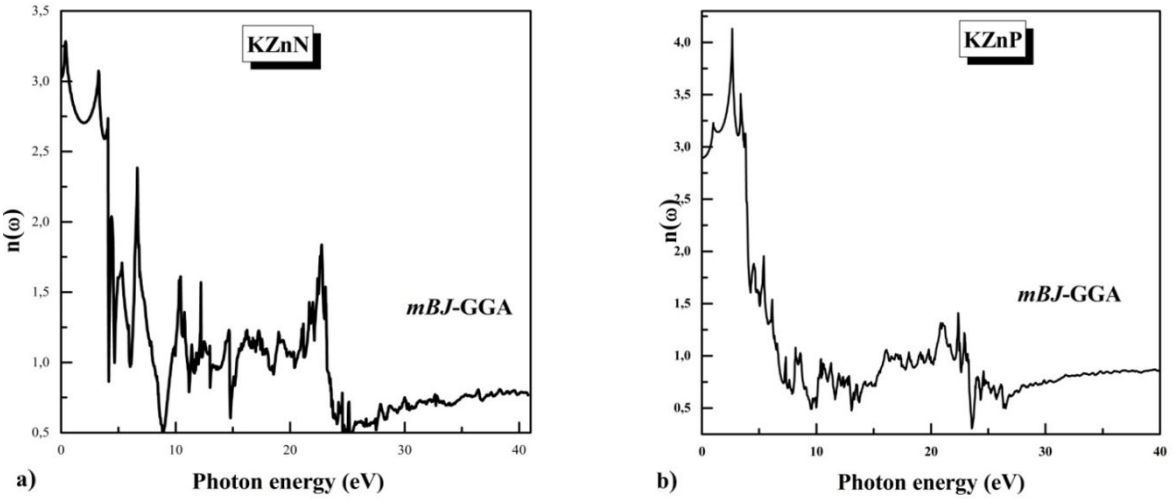

FIGURE 9. Refractive index $n(\omega)$ for a) KZnN and b) KZnP compounds.

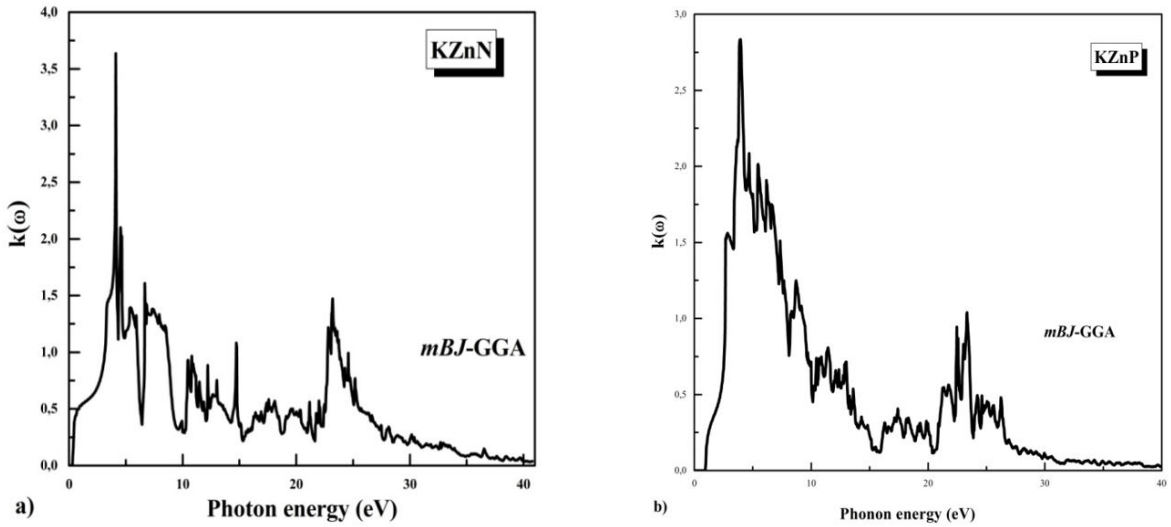

FIGURE 10. Extinction coefficient $K(\omega)$ for a) KZnN and b) KZnP compounds.

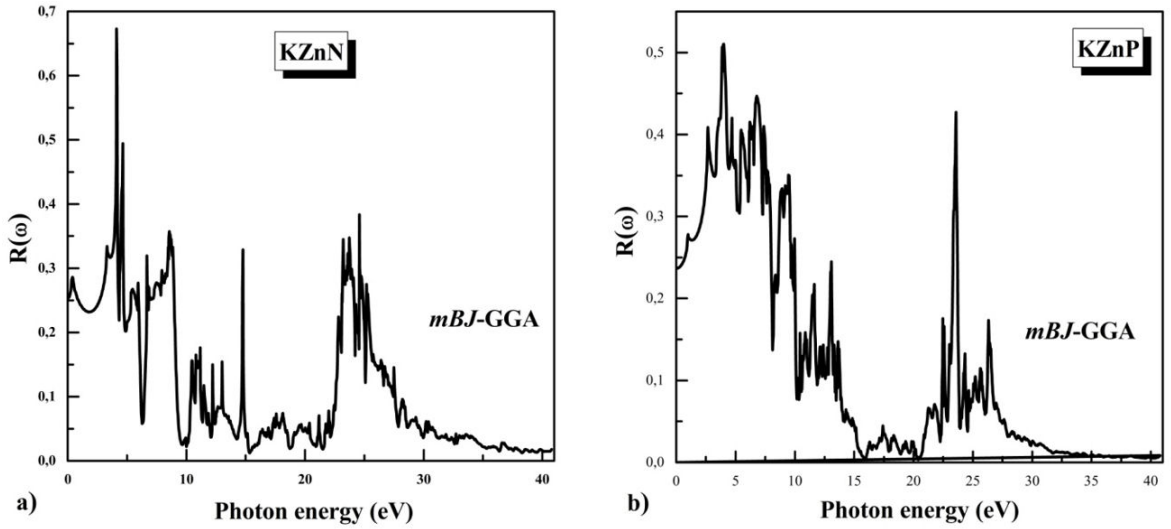

FIGURE 11. The spectral variation of the reflectivity $R(\omega)$ for KZnN and KZnP compounds.

reflectivity $R(0)$ corresponding to an almost zero frequency equals 0.253 for KZnN and 0.237 for KZnP. Also, reflectivity curves of two compounds can be divided in two regions:

i In the 1st region, between 0 eV and 20.45 eV, there are several peaks for two compounds, the highest is at 4.08 eV, reaching a percentage of 68% for KZnN, while for KZnP, the highest one is at 3.99 eV, reaching a percentage 51%.

ii The 2nd region, between 20.45 eV and 40 eV, there are several less intense peaks, the highest is at 24.62 eV for KZnN that corresponds to reflectivity rate, 38.27% as for KZnP, the highest peak is at 23.60 eV with a reflectivity rate, 42.68%. Then the curve decreases for both materials and tends beyond 32 eV. The maximum reflectivity therefore occurs in the ultraviolet and visible domains for KZnN and KZnP compounds.

The values of static dielectric function, $\varepsilon_1(0)$, refractive index $n(0)$ and reflectivity $R(0)$ for KZnN and KZnP half-Heusler compounds have been listed in Table VII. The results verify the condition $n(0) = \sqrt{(\varepsilon_1(0))}$ that results from Eq. (14), and close to theoretical results [20,23].

3.3.3.4 The absorption coefficient

The frequency dependent absorption coefficient is defined as a part of energy of incident ray, which is absorbed in a unit length of crystal, it can be calculated by:

$$\alpha(\omega) = 2\omega k(\omega). \tag{16}$$

The absorption coefficient $\alpha(\omega)$ depends on imaginary part of complex refractive index. From the curves illustrated

TABLE VII. The static dielectric function ε, refractive index n and reflectivity R for the half-Heusler KZnN and KZnP compounds at zero frequency.

	Study	Approximation	$\varepsilon(0)$	$n(0)$	$R(0)$
KZnN	Present work	mBJ-GGA	9.152	3.025	0.253
	Other. theo.	TB-mBJ	8.820[a]	2.790[a]	
		GGA	7.644[c]	2.761[c]	
KZnP	Present work	mBJ-GGA	8.379	2.895	0.237
	Other. theo.	GGA	7.472[c]	2.733[c]	

[a]Ref. [20], [c]Ref. [23].

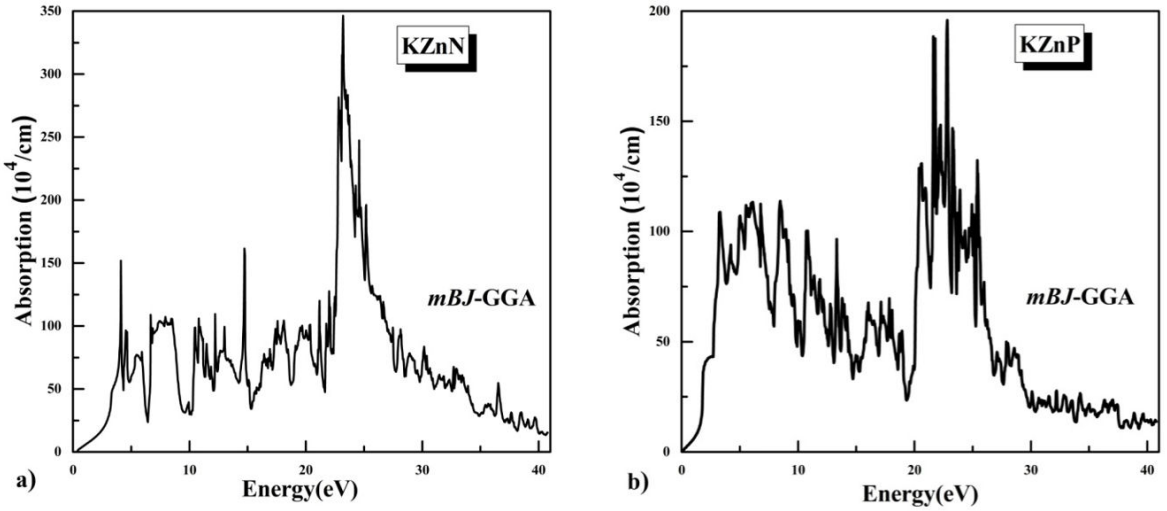

FIGURE 12. Absorption coefficient of a) KZnN and b) KZnP compounds.

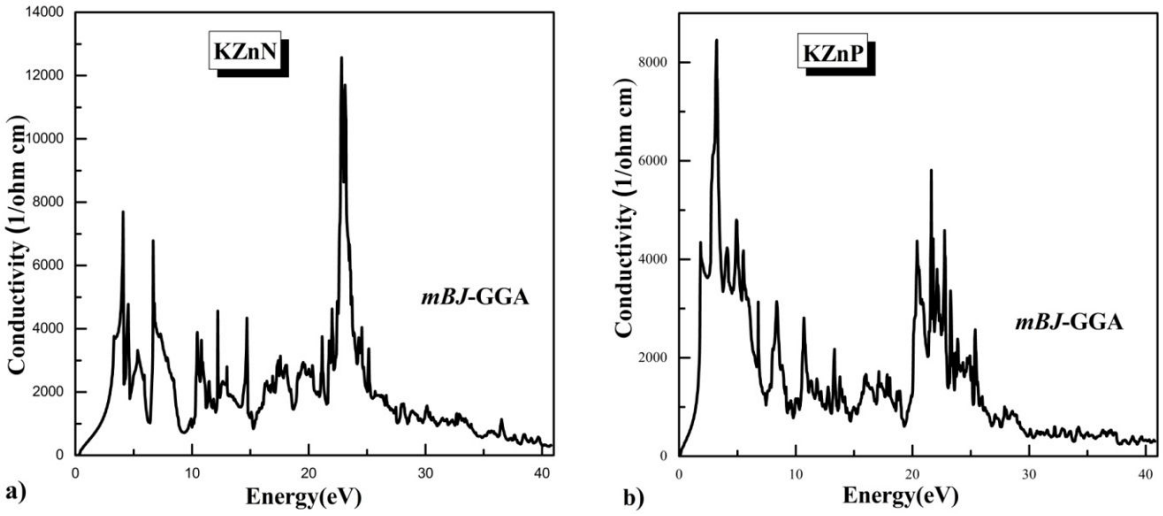

FIGURE 13. Conductivity of for a) KZnN and b) KZnP compounds.

in Figs. 12a), b), it can be seen that two materials have a similar appearance, which consists of two distinct regions:

1. The first region that ranges between 0 and 20 eV has several peaks of light absorption. It is highest peak reaches an absorption maximum, 159.32 104 cm^{-1} for KZnN and 113.22 49 104 cm^{-1} for KZnP. The absorption fluctuates and reaches a minimum value, 27.14 104 cm^{-1} at 6.34 eV for KZnN, and a minimum value, 25.43 104 cm^{-1} at 19.36 eV for KZnP.

2. In the second region, the absorption increases rapidly, presenting several peaks, until reaching a maximum peak, 344.27 104 cm^{-1} that corresponds to 23.33 eV for KZnN and a maximum peak, 194.70 104 cm^{-1} that corresponds to 22.85 eV for KZnP, and finally the curves gradually decrease until the minimum value, 14.67 104 cm^{-1} for KZnN and 13.48 104 cm^{-1} for KZnP.

The high absorption peaks of the two compounds correspond to ultraviolet domain, The wavelengths of KZnN and KZnP compounds that correspond to maximum peaks are 53.3 nm and 54.4 nm, respectively.

3.3.3.5 Conductivity

The measurable amount of optical reflecting substance and character of dependent frequency are estimated and described accordingly by the factor of optical conductivity; this factor is a complex quantity that is given by:

$$\sigma(\omega) = n(\omega)\alpha(\omega)\frac{\omega}{2\pi}, \tag{17}$$

where $n(\omega)$ and $\alpha(\omega)$ are refractive index and absorption coefficient, respectively. Figure 13a), b) represents the spectrum of conductivity for KZnN, the curve presents moderate peaks of conductivity highest being 7755.298 $ohm^{-1}cm^{-1}$ at 4.123 eV then decreases. Above 20 eV, the curve increases sharply until reaching a greater peak, 12567.1 $ohm^{-1}cm^{-1}$ at 22.817 eV, then it decreases at same pace, after 25 eV, it continues to slowly decreasing towards 0. For KZnP, the curve shows multiple peaks of conductivity highest being 8453.14 $ohm^{-1}cm^{-1}$ at 3.225 eV, then it decreases presenting several small peaks until reaching a minimum value, 663.30 $ohm^{-1}cm^{-1}$, then the curve goes back up reaching a peak of 5804.91 $ohm^{-1}cm^{-1}$ that is relatively smaller to highest one, then it decreases gradually until stabilizing towards 307.80 $ohm^{-1}cm^{-1}$. To highlight the importance of various factors in achieving optoelectronic studies, it has suggested potential avenues for further improvement [47-53].

4. Conclusions

This study has allowed us to increase our knowledge on the structural, mechanical, electronic and optical properties of half-Heusler KZnN and KZnP compounds. Using the full potential linearized augmented plane wave method (FP-LAPW), implemented in Wien-2K code, the main characteristics of these materials have been determined. Starting by determining the most stable structure among the three types of arrangements, the results obtained on the structural parameters (the mesh parameter, the compression modulus and its derivative), turned out to be quite close to the theoretical results found in the literature. We have verified the mechanical stability of both materials by ensuring that the calculated elastic constants satisfy the cubic stability criteria of structure type I. Our findings show that KZnN is a ductile material and considerably stiffer than KZnP, which exhibits brittleness. From the band structure, with using mBJ-GGA, a direct gap in Γ has been determined for the two compounds, which proves their semiconductor character. The behavior of important optical parameters was analyzed for a wide range between 0 eV and 40 eV, static and critical energy points were also determined, it is found that the absorption is maximum in the ultraviolet domain for KZnN and KZnP, and the maximum reflectivity also occurs in the ultraviolet domain, and more moderately in the visible domain. Thus, these compounds can serve as viable ultraviolet absorbers as well as radiation protection materials, in particular over wide energy ranges, hoping that future experimental studies will help to validate these hypotheses.

Conflict of interest

The authors declare that they have no conflict of interest.

1. T. Graf, C. Felser, S.S.P. Parkin, Simple rules for the understanding of Heusler compounds. *Prog. Solid. State Ch.* **39** (2011) 1-50, https://doi.org/10.1016/j.progsolidstchem.2011.02.001.
2. F. Heusler, *Verh. Dtsch. Phys. Ges.* **5** (1903) 219.
3. D. Bang, N.H. Dan, N.A. Tuan, and N. X. Phuc, Magnetic and transport properties of Cu2MnAl Heusler alloy prepared by rapidly quenched method. *J. Magn. Magn. Mater.* **310** (2007) 48, https://doi.org/10.1016/j.jmmm.2006.07.027.
4. K. Aniruddha Deb and Y. Sakurai, Electronic structure of the Cu2MnAl Heusler alloy, *J. Phys.: Condens. Matter* **12** (2000) 2997, https://iopscience.iop.org/0953-8984/12/13/310.
5. L. Feng, E.K. Li, W.X. Zhang, W.H. Wang, and G.H. Wu, First-principles investigation of half-metallic ferromagnetism of half-Heusler compounds XYZ. *J. Magn. Magn.* **351** (2014) 92, https://dx.doi.org/10.1016/j.jmmm.2013.09.054.
6. Y. Nishino, M. Kato, S. Asano, K. Soda, M. Hayasaki, and U. Mizutani, Semiconductor like Behavior of Electrical Resistivity in Heusler-type Fe2VAl Compound. *Phys. Rev. Lett*, **79** (1997) 1909, https://id.nii.ac.jp/1476/00004507.
7. J. Winterlik, G.H.Fecher, A. Thomas and C. Felser, Superconductivity in palladium-based Heusler compounds, *Phys. Rev. B* **79** (2009) 064508, https://doi.org/10.1103/PhysRevB.79.064508.
8. H. Itoh, T. Nakamichi, Y. Yamaguchi and N. Kazama. Neutron Diffraction Study of Heusler Type Alloy $Mn_{0.47}V_{0.28}Al_{0.25}$. *Trans. Japan. Inst. Met*. **24** (1983) 265.

9. H. Nakamura, Y. Kitaoka, K. Asayama, Y. Onuki, and T. Komatsubara, *J. Magn. Magn. Mater,* **76** (1988) 466.
10. R.A. de Groot, F.M. Mueller, P.G.van Engen and K.H.J. Buschow, New Class of Materials: Half Metallic Ferromagnets, *Phys. Rev. Lett*, **50** (1983) 2024.
11. M. Gilleßen and R. Dronskowski, A Combinatorial Study of Full Heusler Alloys by First-Principles Computational Methods, *J. Comput. Chem.* **30** (2009) 1290, https://doi.org/10.1002/jcc.21152.
12. K. Özdoğan, E. Şaşloğlu, and I. Galanakis, Antiferromagnetic half-metals, gapless half-metals, and spin gapless semiconductors: The D03-type Heusler alloys, *J. Appl. Phys.* **113** (2013) 193903, https://doi.org/10.1063/1.4840318.
13. M. Ayad *et al*., First-principles calculations to investigate magnetic and thermodynamic properties of new multifunctional full-Heusler alloy Co2TaGa. *Indian J. Phys.* **94** (2020) 767, https://doi.org/10.1007/s12648-019-01518-3.
14. I. Galanakis, P. Mavropoulos, and P. H. Dederichs, Electronic structure and Slater-Pauling behaviour in half-metallic Heusler alloys calculated from first principles, *J. Phys D: Appl. Phys.* **39** (2006) 765, https://doi.org/10.1088/0022-3727/39/5/S01.
15. T. Gruhn, Comparative ab initio study of half-Heusler compounds for optoelectronic applications, *Phys. Rev. B.* **82** (2010) 125210, https://doi.org/10.1103/PhysRevB.82.125210.
16. F. Benzoudji *et al*., Insight into the structural, elastic, electronic, thermoelectric, thermodynamic and optical properties of MRhSb (M=Ti, Zr, Hf) half-Heuslers from ab initio calculations. *Chin. J. Phys.* **59** (2019) 434, https://doi.org/10.1016/j.cjph.2019.04.009.
17. N. Belmiloud, F. Boutaiba, A. Belabbes, M. Ferhat, and F. Bechstedt, Half-Heusler compounds with a 1 eV (1.7 eV) direct band gap, lattice-matched to GaAs (Si), for solar cell application: A first-principles study. *Phys. Status Solidi B* **253** (2016) 889, https://doi.org/10.1002/pssb.201552674.
18. W. Kohn and L. J. Sham, Self-Consistent Equations Including Exchange and Correlation Effects. *Phys. Rev.* **140** (1965) 1133, https://10.1103/physrev.140.a1133.
19. T. Gruhn, Comparative ab initio study of half-Heusler compounds for optoelectronic applications. *Phys. Rev. B* **82** (2010) 125210, https://doi.org/10.1103/PhysRevB.82.125210.
20. S. Kacimi, H. Mehnane, and A. Zaoui, I-II-V and I-III-IV half-Heusler compounds for optoelectronic applications: Comparative ab initio study. *Journal of Alloys and Compounds* **587** (2014) 451, https://doi.org/10.1016/j.jallcom.2013.10.046.
21. D. Kieven, R. Lenk, S. Naghavi, C. Felser and T. Gruhn, I-II-V half-Heusler compounds for optoelectronics: Ab initio calculations. *Phys. Rev. B.* **81** (2010) 075208, https://doi.org/10.1103/PhysRevB.81.075208.
22. J. Liu, Y. Zhao, C. Lian, Z. Dai, J.-Tao Sun and S. Meng, Ab initio study on anisotropic thermoelectric transport in ternary pnictide KZnP. *J. Phys.: Mater.* **2** (2019) 024001, https://doi.org/10.1088/2515-7639/ab05ea.
23. H. Mehnane, B. Bekkouche, S. Kacimi, A. Hallouche, M. Djermouni, A. Zaoui, First-principles study of new half Heusler for optoelectronic applications. *Superlattices Microstruct.* **51** (2012) 772, https://doi.org/10.1016/j.spmi.2012.03.020.
24. A.E. Carlsson, A. Zunger, D.M. Wood, Electronic structure of LiZnN: Interstitial insertion rule. *Phys. Rev. B* **32** (1985) 1386, https://doi.org/10.1103/physrevb.32.1386.
25. H.J.F. Jansen and A.J. Freeman, Total -energy full-potential linearized augmented -plane -wave method for bulk solids: Electronic and structural properties of tungsten. *Phys. Rev. B.* **30** (1984) 561.
26. P. Blaha, K. Schwarz, G.K.H. Madsen, D. Kvasnicka and J. Luitz, Vienna University of Technology, Vienna, 2001.
27. K. Schwarz and P. Blaha, Solid state calculations using wien2k. *Comput. Mater. Sci.* **28** (2003) 259, https://doi.org/10.1016/S0927-0256(03)00112-5.
28. J.P. Perdew, S. Burke, and M. Ernzerhof, Generalized Gradient Approximation Made Simple. *Phys. Rev. Lett.* **77** (1996) 3865, https://doi.org/10.1103/physrevlett.77.3865.
29. F. Tran and P Blaha, Accurate Band Gaps of Semiconductors and Insulators with a Semilocal Exchange-Correlation Potential. *Phys. Rev. Lett.* **102** (2009) 226401, https://dx.doi.org/10.1103/PhysRevLett.102.226401.
30. H.J. Monkhorst and J.D. Pack, Special points for Brillouin-zone integrations. *Phys. Rev. B* **13** (1976) 5188, https://doi.org/10.1103/PhysRevB.13.5188.
31. F.D. Murnaghan, The compressibility of media under extreme pressures. *Proc. Natl. Acad. Sci. USA.* **30** (1944) 5390.
32. Z. Naturforsch, On Ternary Pnictides and Chalkogenides of Alkaline Metals and IB-resp. *II B-Elements, 33b* (1978) 370, https://doi.org/10.1515/znb-1978-0404
33. M.J. Mehl, Pressure dependence of the elastic moduli in aluminum-rich Al-Li compounds, *Phys. Rev. B: Condensed Matter* **47** (1993) 2493, https://doi.org/10.1103/PhysRevB.47.2493.
34. E. Schreiber, O.I. Anderson, N. Soga, Elastic Constants, and Their Measurements, McGraw-Hill Companies, Inc., (New York, 1973).
35. M. Born and K. Huang, Dynamical Theory of Crystal Lattice (Oxford: Oxford University Press) (1954).
36. VS.F. Pugh, XCII. Relations between the elastic moduli and the plastic properties of polycrystalline pure metals. Lond. Edinb. Dublin Philos. *Mag. J. Sci*. **45** (1954) 823, https://doi.org/10.1080/14786440808520496.
37. M. J. Mehl, B. K. Klein and D. A. Papa, Constantopoulos Intermetallic Compounds Principle and Practice. Principles. I. (eds.) J H Westbrook and R L Fleischeir (Hoboken: Wiley) (1995).
38. W. Voigt Lehrbush Der Kristall physik (Leipzig: Taubner) (1928).
39. J. Haines, J. M. Leger and G. Bocquillon, Synthesis and Design of Superhard Materials. *Annu. Rev. Mater. Res.* **31** (2001) 1, https://doi.org/10.1146/annurev.matsci.31.1.1.

40. L. Ai and X. L. Gao, Metamaterials with negative Poisson's ratio and non-positive thermal expansion, *Compos. Struct.* **162** (2017) 70. https://dx.doi.org/10.1016/j.compstruct.2016.11.056.
41. C. F. Bohren, D. R. Huffman, Absorption and Scattering of light by small particles, Wiley-Interscience, New-York, (1983).
42. G. Harbeke, In Optical properties of solids (Ed: F. Abelès), North-Holland, Amsterdam (1972), 23
43. C. Kittel, Physique de l'état solide, 5éme ed., Bordas, Paris, (1983)
44. H. Ehrenreich and H. Philips, Optical properties of Ag and Cu. *Phys. Rev.* **128** (1962) 1622.
45. L. Lew, Y. Voon, and L. Ram-Mohan, Tight-binding representation of the optical matrix elements: Theory and applications. *Phys. Rev. B* **47** (1993) 15500, https://doi.org/10.1103/PhysRevB.47.15500.
46. D. Allali *et al*., Electronic and optical properties of the SiB2O4 (B=Mg, Zn, and Cd) spinel oxides: An ab initio study with the Tran-Blaha-modified Becke-Johnson density functional, *Physica B* **443** (2014) 24, https://doi.org/10.1016/j.physb.2014.02.053.
47. A. Fouad *et al*., Optical properties of GaX (X=P, As, Sb) under hydrostatic pressure, *Experimental and Theoretical Nanotechnology* **7** (2023) 283, https://doi.org/10.56053/7.2.283.
48. N. Kojal, S. Javec, Structuraland thermal properties of H6Ta2O17, *Experimental and Theoretical Nanotechnology* **7** (2023) 309, https://doi.org/10.56053/7.2.309.
49. V. Raman, and A. Rajan, Thermodynamic properties of MgFeH3 alloy, *Experimental and Theoretical Nanotechnology* **7** (2023) 381, https://doi.org/10.56053/7.2.381.
50. S. Radiman, and M. Rusop, Investigation of structural and optical properties of In-doped AlSb nanostructures, *Experimental and Theoretical Nanotechnology* **7** (2023) 49, https://doi.org/10.56053/7.1.49.
51. O. Jabbar and A. H. Reshak, Structural, electronic, and optoelectronic properties of XYZ2 (X=Zn,Cd; Y=Si,Sn;Z=pnicogens) Chalcopyrite compounds: First-principles calculations, *Experimental and Theoretical Nanotechnology* **7** (2023) 97, https://doi.org/10.56053/7.1.97.
52. J. Liu, and R. Yang, Structural, dynamical, thermodynamic properties of CdYF3 perovskite, *Experimental and Theoretical Nanotechnology* **7** (2023) 111, https://doi.org/10.56053/7.1.111.
53. R. Sahnoun, Gap bowing of in Pb1-xCaxS, Pb1-xCaxSe and Pb1-xCaxTe alloys, *Experimental and Theoretical Nanotechnology* **7** (2023) 149, https://doi.org/10.56053/7.1.149.